Letters in Applied NanoBioScience
Open-Access Journal (ISSN: 2284-6808)

Article
Volume 15, Issue 1, 2026, 5
https://doi.org/10.33263/LIANBS151.005

Effect of Heat Transfer on Radiative MHD Micropolar Fluid Flow over a Stretching Inclined Sheet in the Presence of Chemical Reaction and Heat Sink/Source

Keshab Borah [1,*], Shyamanta Chakraborty [2], Jadav Konch [1], Salma Akhtar [3]

[1] Department of Mathematics, Dhemaji College, Assam, 787057, India
[2] UGC-MMTTC, Gauhati University, Guwahati, Assam, India
[3] Department of Mathematics, Gauhati University, Guwahati, Assam, India
* Correspondence: keshabborah@dhemajicollege.in

Received: 11.10.2025; Accepted: 2.02.2026; Published: 30.03.2026

Abstract: This study examines the steady, two-dimensional magnetohydrodynamic (MHD) boundary-layer flow and heat transfer of a micropolar fluid over an exponentially stretching inclined sheet. The analysis incorporates the effects of viscous dissipation, Joule heating, thermal radiation, a porous medium, a chemical reaction, a heat source/sink, and velocity slip. The nonlinear partial differential equations governing the flow are converted into ordinary differential equations through similarity transformations and solved numerically using MATLAB's bvp4c solver. The numerical solution demonstrates reliable convergence and accuracy, confirmed through comparison with published benchmark data. The numerical results for velocity, angular velocity, temperature, and concentration are presented graphically, and the influence of various parameters, including the Chemical Reaction Parameter, Porosity Parameter, Eckert Number, Thermal Radiation Parameter, and heat source parameter, is analyzed. Results indicate that Eckert number, thermal radiation parameter, and chemical reaction parameter significantly elevate the thermal boundary layer thickness. Conversely, higher porosity parameters reduce temperature and concentration profiles. Further, skin friction, Nusselt number, and Sherwood number demonstrate clear sensitivity to melting effects. Findings from this work provide insights relevant to industrial processes involving polymer extrusion, thermal insulation systems, porous media transport, and heat-assisted chemical reactors.

Keywords: micropolar fluid; melting heat transfer; Joule heating; thermal radiation; chemical reaction.

1. Introduction

The study of micropolar fluid flow has gained significant momentum in recent decades due to its extensive applications in various engineering and industrial processes. Micropolar fluids, first introduced by Eringen in the mid-1960s, represent a class of non-Newtonian fluids characterized by their ability to exhibit micro-rotational effects and support couple stresses. Unlike conventional Newtonian fluids, Micropolar fluids are composed of rigid, randomly oriented particles dispersed within a viscous medium, making them particularly suitable for modeling complex fluids such as blood, liquid crystals, and polymeric suspensions [1,2].

The incorporation of magnetohydrodynamic (MHD) effects, thermal radiation, chemical reactions, and heat source/sink phenomena in micropolar fluid flow analysis has become increasingly important for understanding complex thermal and mass transfer mechanisms in engineering applications.

Stretching sheet problems in micropolar fluid flow have gained considerable attention due to their relevance in manufacturing processes such as polymer extrusion and fiber spinning. Crane [3] initiated the examination of boundary-layer flow along stretching sheets, laying the essential foundation that later researchers expanded to study micropolar fluids. Agrawal *et al*. [4] conducted a study analyzing the melting heat transfer and flow dynamics of a micropolar fluid induced by an exponentially stretching sheet. Their investigation considered the coupled effects of slip parameters, viscous dissipation, Joule heating, internal heat sources, and thermal radiation. Sharma *et al*. [5] investigated the heat and mass transfer phenomena in MHD micropolar fluids influenced by a permeable and continuously stretching sheet, incorporating slip effects within a porous medium. Borah *et al*. [6] investigated the effects of Soret and Dufour phenomena along with chemical reactions on the flow of gyrotactic microorganisms and micropolar nanofluid over a stretching/shrinking sheet, considering the influences of radiation, viscous dissipation, a uniform magnetic field, and a heat source. Abdelgaber *et al*. [7] analyzed the flow of heat & mass transfer in a micropolar fluid past a stretching sheet, subjected to an external magnetic field, thermal radiation, and chemical reaction.

Thermal radiation plays a crucial role in micropolar fluid heat transfer, particularly at high temperatures where radiative heat flux becomes significant. Lu *et al*. [8] examined the influence of nonlinear thermal radiation on micropolar nanofluid flow over vertically extending surfaces, taking into account magnetohydrodynamics, heat generation/absorption, and mixed convection effects. A study into the effects of radiation on the incompressible convective-thermos transmission of micropolar fluid over an extensible permeable sheet with mass and energy conversion was given by Bilal *et al*. [9]. Kausar *et al*. [10] analyzed the influence of thermal radiation and viscous dissipation on stagnation-point flow of a micropolar fluid past a permeable stretching sheet. Saraswathy *et al*. [11] investigated the coupled effects of nonlinear thermal radiation, viscous dissipation, and magnetic field on MHD micropolar fluid flow through a porous medium. Shamshuddin *et al*. [12] analyzed the effects of thermal radiation and chemical reactions on the transport behavior of micropolar nanofluid flow along a vertical sheet adjacent to an isothermal porous structure.

Mohapatra *et al*. [13] investigated the role of chemical reactions in MHD micropolar fluid flow over vertical surfaces through a porous medium with internal heat sources. Singh and Kumar [14] analyzed how chemical reactions impact the heat and mass transfer in micropolar fluid flow through permeable channels that involve radiation and heat generation. They applied the Rosseland approximation to model radiative heat flux and established that the parameters related to chemical reactions notably influence the thickness of the concentration boundary layer. Verma *et al*. [15] conducted a numerical investigation of chemical reactions in magnetohydrodynamic (MHD) micropolar fluid flows at stagnation points, incorporating the effects of nanoparticles and external heat sources.

Mukhopadhyay [16] has studied the slip effect on the magnetohydrodynamic (MHD) boundary layer flow over an exponentially stretching plate, considering the influences of thermal radiation, suction, and blowing. Ramzan *et al*. [17] investigated the motion of a micropolar fluid across a permeable, stretched sheet, accounting for Joule heating, thermal radiation, partial slip, and magnetohydrodynamics (MHD) under convective boundary conditions. In their study, Mandal *et al*. [18] analyzed how velocity slip and thermal radiation influence the magnetohydrodynamic flow and melting heat transfer of a micropolar fluid along an exponentially stretching sheet. An investigation into the simultaneous effects of electromagnetic force, chemical reaction, and thermal radiation on Oldroyd-B fluid flow across an exponentially stretched sheet embedded in a porous medium with a heat sink was conducted by Salah and Sidahmed [19]. Naim *et al*. [20] analyzed the magnetohydrodynamic stagnation-point flow and thermal characteristics of a micropolar fluid over an exponentially stretching sheet or shrinking vertical sheet, considering convective boundary conditions and buoyancy effects.

The study provides a comprehensive numerical investigation, using bvp4c, of how key parameters, including the Hartmann number, material and porosity parameters, Eckert number, radiation and heat-source parameters, Schmidt number, and chemical-reaction parameter jointly influence velocity, microrotation, temperature, concentration, and related engineering quantities such as skin friction, couple stress, and Nusselt and Sherwood numbers. It establishes new benchmark data by validating limiting cases against Ibrahim *et al*. [21], before extending the analysis to a broader micropolar, radiative, chemically reactive, porous, and melting regime not previously explored. Addressing a clear research gap, the work incorporates physical effects typically omitted in earlier MHD micropolar studies—such as porous-medium resistance, Joule heating, viscous dissipation, chemical reaction, sheet inclination, and melting—and becomes the first to present results for radiative MHD micropolar flow over an exponentially stretching inclined melting sheet with simultaneous slip, heat generation/absorption, and chemical reaction, thereby generalizing several earlier configurations into a single framework.

2. Problem Formulation

We have considered the two-dimensional motion of a micropolar fluid, both incompressible and electrically conducting, moving steadily over an exponentially stretching inclined sheet that is melting at a stable rate. A variable magnetic field $B(x) = B_0 e^{\frac{x}{2L}}$ is applied perpendicular to the direction of motion, where B_0 represents a constant. Since the magnetic Reynolds number is low, the induced magnetic field can be ignored when compared to the applied magnetic field. Let us assume $u_e(x) = ae^{\frac{x}{L}}$ be the free stream velocity and $u_w(x) = be^{\frac{x}{L}}$ that the exponential velocity when the surface is stretched, with a and b being real constants, the x-axis runs along the continuous stretching surface, whereas the y-axis is perpendicular to the surface.

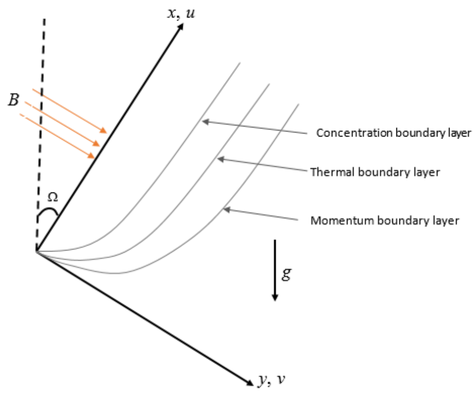

Figure 1. Physical geometry of the flow.

The thermal energy expression takes into account the effects of radiation, Joule heating, and viscous dissipation. Additionally, the flow at the stagnation point is also being considered. Figure 1 shows the setup of the model along with the coordinate system.

The governing equations that depict flow under these assumptions are as follows:

$$\frac{\partial u}{\partial x}+\frac{\partial v}{\partial y}=0 \tag{1}$$

$$u\frac{\partial u}{\partial x}+v\frac{\partial u}{\partial y}=u_e\frac{du_e}{dx}+\left(\frac{\mu+\kappa}{\rho}\right)\frac{\partial^2 u}{\partial y^2}+\frac{\kappa}{\rho}\frac{\partial N}{\partial y}-\frac{\sigma {B_0}^2 u}{\rho}-\frac{v}{k_p'}+g[\beta_T(T-T_\infty)+\beta_C(C-C_\infty)]\cos\Omega \tag{2}$$

$$u\frac{\partial N}{\partial x}+v\frac{\partial N}{\partial y}=\frac{\gamma}{\rho j}\frac{\partial^2 N}{\partial y^2}-\frac{\kappa}{\rho j}\left(2N+\frac{\partial u}{\partial y}\right) \tag{3}$$

$$u\frac{\partial T}{\partial x}+v\frac{\partial T}{\partial y}=\frac{k}{\rho C_p}\frac{\partial^2 T}{\partial y^2}-\frac{1}{\rho C_p}\frac{\partial q_r}{\partial y}+\left(\frac{\mu+\kappa}{\rho C_P}\right)\left(\frac{\partial u}{\partial y}\right)^2+\frac{\sigma B_0^2}{\rho C_p}u^2+\frac{Q_0}{\rho C_P}(T-T_\infty) \tag{4}$$

$$u\frac{\partial C}{\partial x}+v\frac{\partial C}{\partial y}=D\frac{\partial^2 C}{\partial y^2}-k_0(C-C_\infty) \tag{5}$$

The Rosseland approximation simplifies Eq. (4), reducing the radiative heat flux to:

$$q_r=-\frac{4\sigma^*}{3k^*}\frac{\partial T^4}{\partial y} \tag{6}$$

Here, σ^* and k^* represent the Stefan-Boltzmann constant and the mean absorption coefficient, respectively. Expanding T^4 around T_∞(the free stream temperature) using a Taylor series and ignoring higher-order terms, we obtain:

$$T^4\cong 4T_\infty^3 T-3T_\infty^4 \tag{7}$$

Hence, Eq. (4) reduces to:

$$u\frac{\partial T}{\partial x}+v\frac{\partial T}{\partial y}=\frac{k}{\rho C_p}\frac{\partial^2 T}{\partial y^2}+\frac{16T_\infty^3\sigma^*}{3k^*k}\frac{\partial^2 T}{\partial y^2}+\left(\frac{\mu+\kappa}{\rho C_P}\right)\left(\frac{\partial u}{\partial y}\right)^2+\frac{\sigma B_0^2}{\rho C_p}u^2+\frac{Q_0}{\rho C_P}(T-T_\infty) \tag{8}$$

The symbols used are as follows: u and v are the velocity components in the x- and y-directions, respectively; σ signifies the electrical conductivity; ρ stands for the density of the fluid ; μ is the fluid's viscosity; κ is the coefficient of vortex viscosity; N is the micro-rotation; $\upsilon=\frac{\mu}{\rho}$ is the kinematic viscosity; $k_p^{'}$ is the Darcy permeability; g is the acceleration due to gravity; β_T and β_C denotes thermal and volumetric expansion coefficient; T, T_m, and T_∞ represent the fluid temperature, melting surface temperature, and free-stream temperature, respectively, where $T_\infty>T_m$; Ω is the angle of inclination; $j=\frac{2Lve^{-\frac{x}{L}}}{a}$ is the micro-inertia density; $\gamma=\left(\mu+\frac{\kappa}{2}\right)j$ is the spin gradient viscosity; k is the thermal conductivity of the fluid, C_p is the specific heat; D is the molecular diffusivity; k_0 denotes the rate constant of a first-order irreversible chemical reaction.

The boundary conditions are given as:

$$\left.\begin{array}{llll} u=u_w+u_{slip}, N=-n\frac{\partial u}{\partial y}, T=T_m, k\frac{\partial T}{\partial y}=\rho[\lambda+c_s(T_m-T_0)]v, C=C_m & at & y=0 \\ u=0, \quad N=0, \quad T=T_\infty, \quad C=C_\infty & as & y\to\infty \end{array}\right\} \tag{9}$$

The slip velocity is expressed as: $u_{slip} = \chi(x)\frac{\partial u}{\partial y}$, $\chi(x) = Ae^{-\frac{x}{2L}}, A, n$ is a constant, λ denotes the fluid's latent heat, and c_s represents the surface heat capacity.

To convert the nonlinear PDEs into nonlinear ODEs, similarity transformations are introduced.

$$\eta = y\sqrt{\frac{a}{2\upsilon L}}e^{\frac{x}{2L}};\ \ \psi = \sqrt{2\upsilon aL}e^{\frac{x}{2L}}f(\eta);\ \ N = \frac{a}{2\upsilon L}\sqrt{2\upsilon aL}e^{\frac{3x}{2L}}h(\eta);\ \ \theta(\eta) = \frac{T-T_\infty}{T_m-T_\infty};$$
$$\phi(\eta) = \frac{C-C_\infty}{C_w-C_\infty}$$

Where $T_m = T_\infty + T_0 e^{\frac{x}{2L}}$; $C_m = C_\infty + C_0 e^{\frac{x}{2L}}$

The stream function $\psi = \psi(x, y)$ is defined as: $u = \frac{\partial\psi}{\partial y}, v = -\frac{\partial\psi}{\partial x}$, which gives

$$u = ae^{\frac{x}{L}} f'(\eta),\ v = -\sqrt{\frac{a\upsilon}{2L}}e^{\frac{x}{2L}}[f(\eta) + \eta f'(\eta)]$$

Using the above similarity transformation equation (1) is automatically satisfied, and equations (2, 3, 8, and 5) are reduced to the following ODEs.

$$(1+K)f''' - 2(f')^2 + ff'' + 2\varepsilon^2 + Kh' - \left(M + \frac{1}{K_p}\right)f' - [(\lambda_1\theta + \lambda_2\phi)\cos\Omega] = 0 \quad (10)$$

$$\left(1 + \frac{K}{2}\right)h'' - K(2h + f'') + fh' - 3f'h = 0 \quad (11)$$

$$\frac{1}{Pr}\left(1 + \frac{4}{3}R\right)\theta'' + S\theta + f\theta' - f'\theta + (1+K)\,Ec\,(f'')^2 = 0 \quad (12)$$

$$\phi'' + Sc(f\phi' - f'\phi - Kc\,\phi) = 0 \quad (13)$$

The boundary conditions (9) were transformed to:

$$\left.\begin{array}{l} f'(\eta) = 1 + \chi f''(\eta), h(\eta) = -nf''(\eta), \Pr f(\eta) + \alpha\theta'(\eta) = 0, \theta(\eta) = 1, \phi(\eta) = 1\ at\ \eta = 0 \\ f'(\eta) = 0, \quad h(\eta) = 0, \quad \theta(\eta) = 0, \quad \phi(\eta) = 0 \quad as \quad \eta \to \infty \end{array}\right\} \quad (14)$$

Here, primes represent differentiation with respect to η; $M = \frac{2L\sigma {B_0}^2}{\rho a}$ is the Hartmann number, $K = \frac{\kappa}{\mu}$ is the material parameter; $\varepsilon = \frac{b}{a}$ represents the velocity ratio parameter; $K_p = \frac{ak'_p e^{\frac{x}{L}}}{2\upsilon L}$ is the porosity parameter, $Pr = \frac{\mu C_p}{k}$ is the Prandtl number, $\lambda_1 = \frac{Gr}{{Re_x}^2}$ is the buoyancy parameter; $Gr = \frac{2g\beta_T(T_m - T_\infty)L^3}{\upsilon^2}$ is the local thermal Grashof number, $\lambda_2 = \frac{Gc}{{Re_x}^2}$ is the solutal buoyancy parameter; $Gc = \frac{2g\beta_C(C_m - C_\infty)L^3}{\upsilon^2}$ is the local solutal Grashof number; $R = \frac{4\sigma^* T_\infty^3}{k^* k}$ is the thermal radiation parameter, $S = \frac{2LQ_0}{\rho a C_p e^{\frac{x}{L}}}$ is the heat absorption or generation parameter, $Ec = \frac{u_w^2}{C_P(T_m - T_\infty)}$ is the Eckert number, $Sc = \frac{\upsilon}{D}$ is the Schmidt number, $Kc = \frac{2Lk_0}{ae^{\frac{x}{L}}}$ is the chemical reaction parameter, $\alpha = \frac{kC_p(T_\infty - T_m)}{\rho[\lambda + c_s(T_m - T_0)]}$ is the melting parameter.

The expressions for the skin friction coefficient (C_f), couple stress coefficient (C_s), Nusselt number (Nu), and Sherwood number (Sh) are provided as follows:

$$C_f = \frac{\tau_w}{\rho u_w^2}, C_s = \left[\left(\mu + \frac{K}{2}\right) j \frac{\partial N}{\partial y}\right]_{y=0}, Nu = \frac{x q_w}{k(T_m - T_\infty)}, Sh = \frac{x q_m}{D(C_m - C_\infty)} \quad (15)$$

Where $\tau_w = \left[(\mu + \kappa)\frac{\partial u}{\partial y} + \kappa N\right]_{y=0}; q_w = -k\left(\frac{\partial T}{\partial y}\right)_{y=0}; q_m = -D\left(\frac{\partial C}{\partial y}\right)_{y=0}$ (16)

Represents the shear stress, and the heat and mass fluxes at the surface, respectively. Substituting Eq. (16) into Eq. (15), we get:

$$C_f = \frac{[1+(1-n)K]f''(0)}{\sqrt{Re_x}}; Re_x C_s = \left(1 + \frac{K}{2}\right) h'(0); \frac{Nu}{\sqrt{Re_x}} = -\theta'(0); \frac{Sh}{\sqrt{Re_x}} = -\phi'(0) \quad (17)$$

Where $Re_x = \frac{axe^{\frac{x}{L}}}{\upsilon}$ represents the local Reynolds number.

3. Methodology

There are significant challenges in solving the nonlinear partial differential equations and associated boundary conditions; thus, a numerical approach is more effective. The equations are reformulated and numerically solved using the bvp4c method, subject to the specified boundary conditions. Boundary value problems can be efficiently solved numerically by first applying a similarity transformation, which converts the original set of nonlinear partial differential equations into a system of first-order ordinary differential equations (ODEs) and establishes the initial conditions. MATLAB’s bvp4c solver is then employed to solve these ODEs numerically.

The dimensionless nonlinear ordinary differential equations (ODEs) (10)–(13), along with the boundary conditions (14) of the confirmed model, are transformed into the following set of first-order ODEs in order to execute MATLAB’s bvp4c solver:

$$f = y_1$$
$$\frac{df}{d\eta} = y_2$$
$$\frac{d^2 f}{d\eta^2} = y_3$$
$$\frac{d^3 f}{d\eta^3} = \frac{dy_3}{d\eta} = \frac{1}{(1+K)}\Big(2(y_2)^2 - y_1 y_3 - 2\varepsilon^2 - K y_5 + \left(M + 1/K_p\right) y_2 + [(\lambda_1 y_6 + \lambda_2 y_8) \cos \Omega]\Big)$$
$$h = y_4$$
$$\frac{dh}{d\eta} = y_5$$
$$\frac{d^2 h}{d\eta^2} = \frac{dy_5}{d\eta} = \frac{1}{(1 + K/2)}[3 y_2 y_4 + K(2 y_4 + y_3) - y_1 y_5]$$
$$\theta = y_6$$
$$\frac{d\theta}{d\eta} = y_7$$

$$\frac{d^2\theta}{d\eta^2} = \frac{dy_7}{d\eta} = \frac{Pr}{(1+4R/3)}[y_2y_6 - Sy_6 - y_1y_7 - (1+K)Ec(y_3)^2]$$
$$\phi = y_8$$
$$\frac{d\phi}{d\eta} = y_9$$
$$\frac{d^2\phi}{d\eta^2} = \frac{dy_9}{d\eta} = Sc(y_2y_8 - y_1y_9 + Kcy_8)$$

The boundary conditions:

$$\left.\begin{array}{llll} y_2(0) = 1 + \chi y_3(0), y_4(0) = -ny_3(0), Pr\, y_1(0) + \alpha\, y_7(0) = 0, & y_6(0) = 1, & y_8(0) = 1 \\ y_2(\infty) = 0, \quad y_4(\infty) = 0\,, & y_6(\infty) = 0, & y_8(\infty) = 0 \end{array}\right\}$$

To integrate the equations, suitable initial estimate values for the missing boundary conditions are chosen, followed by the integration procedure.

4. Results and Discussion

The nonlinear ordinary differential equations (10)–(13) with boundary conditions (14) are solved numerically using MATLAB's bvp4c solver. The system consists of equations that are third order in f, second order in h, θ, and ϕ. These higher-order ODEs are first reduced to a system of simultaneous first-order ODEs for numerical solution.

To ensure the credibility and robustness of the numerical procedure, the present results were quantitatively validated by comparing the computed values of the temperature gradient $(-\theta'(0))$ with benchmark data mentioned in the literature. The comparison was performed under identical physical conditions in the absence of thermal radiation, slip, heat source/sink, and chemical reaction effects. Table 1 presents a representative comparison between the present simulation and previously published results, demonstrating close agreement. The computed deviation for all cases remained below 0.02%, indicating the high accuracy, numerical stability, and convergence reliability of the employed MATLAB `bvp4c` solver. This negligible deviation confirms that the implemented numerical scheme is suitable for further parametric investigation.

Table 1. Comparison of the $-\theta'(0)$ values for an ordinary viscous fluid ($K = 0$) for selected governing parameters in the absence of thermal radiation, external heat source, slip at the boundary, and chemical reaction.

Magnetic parameter (M)	Prandtl Number (Pr)	Mandal *et al.* [18]	Ibrahim *et al.* [21]	Present Study	% Deviation
0	1	0.95475	0.954749	0.9548	0.0053%
	2	1.47148	1.471478	1.4715	0.0015%
	3	1.86907	1.869069	1.8692	0.0070%
	5	2.50011	2.50010	2.5002	0.0040%
	10	3.66036	3.660358	3.6605	0.0039%
1	1	0.86105	0.861001	0.8611	0.0115%

The graphical representations of the velocity, temperature, concentration, and micro-rotation profiles for various parameters influencing the equations are illustrated in Figures 2-19. These figures demonstrate how different physical and flow parameters affect the profiles.

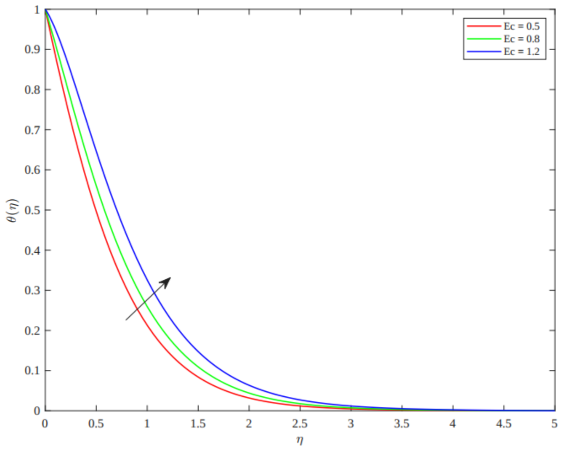

Figure 2. Temperature profile for different Ec values.

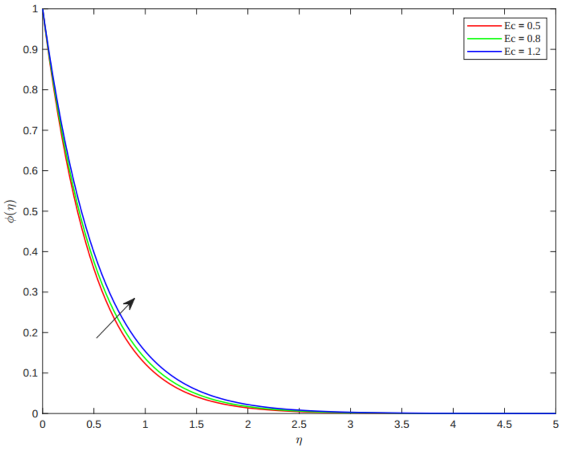

Figure 3. Concentration profile for different Ec values.

The effect of the Eckert number Ec on temperature and concentration profiles is analyzed in Figures 2 and 3. The Eckert number (Ec) relates kinetic energy converted to internal thermal energy through viscous dissipation. It shows that both temperature and concentration profile rise with the Eckert number. As Ec increases, more kinetic energy is transformed into internal energy through viscous dissipation, resulting in greater thermal energy within the fluid. This causes the temperature to rise because higher molecular collisions and friction generate more heat in the boundary layer. An increase in Ec physically implies more conversion of kinetic energy to heat, raising fluid temperature and concentration, as molecular collisions generate additional heat in the boundary layer.

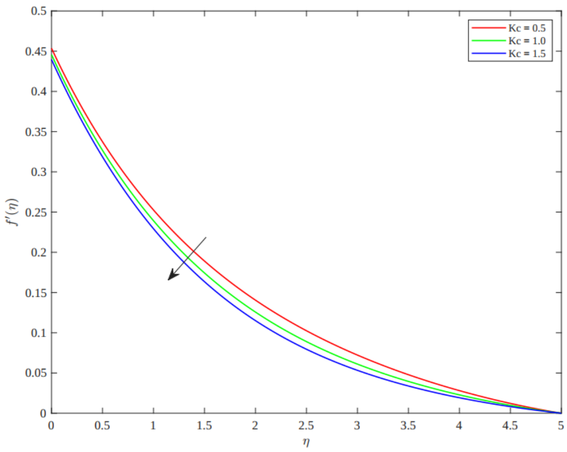

Figure 4. Velocity profile for different Kc values.

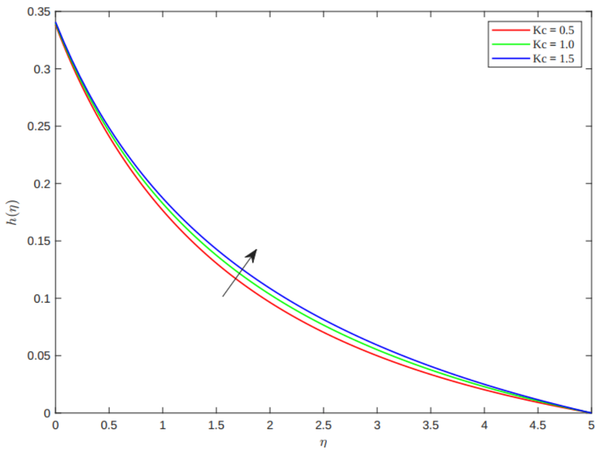

Figure 5. Micro-rotation profile for different Kc values.

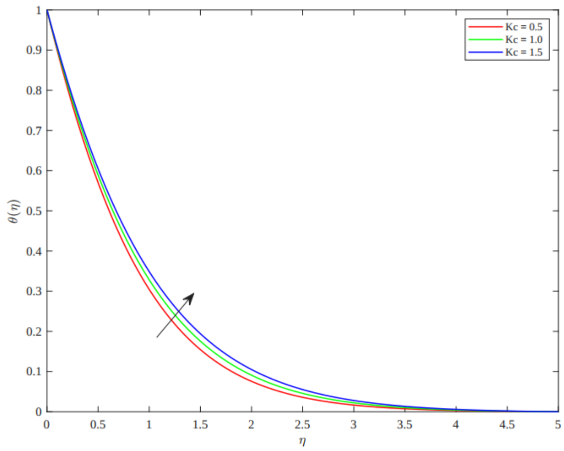

Figure 6. Temperature profile for different Kc values.

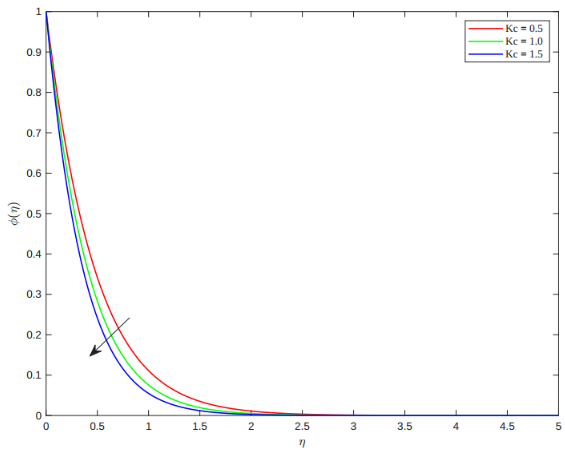

Figure 7. Concentration profile for different Kc values.

Figures 4 to 7 demonstrate how variations in the chemical reaction parameter (Kc) affect the velocity (Figure 4), angular velocity (Figure 5), temperature (Figure 6), and concentration (Figure 7) profiles. The chemical reaction parameter (*Kc*) represents the rate of consumption or generation of chemical species. It is found in Figure 4 that the fluid velocity decreases as the chemical reaction parameter increases. Figures 5 and 6 show that both angular velocity and temperature profiles increase with Kc. The temperature increases with the chemical reaction parameter because the chemical energy generated by the reactions is effectively converted into thermal energy, which heats the fluid and raises its temperature. Figure 7 shows that the concentration profile decreases with Kc. This occurs because the chemical reaction consumes the chemical species within the fluid, leading to a reduction in the concentration profile.

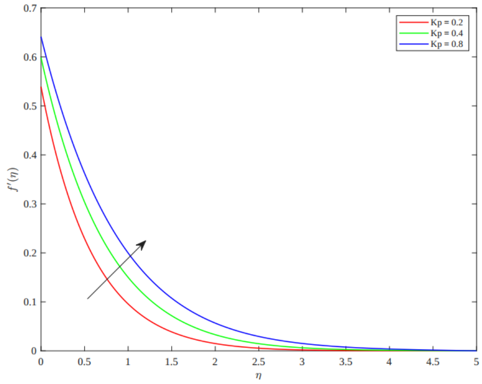

Figure 8. Velocity profile for different Kp values.

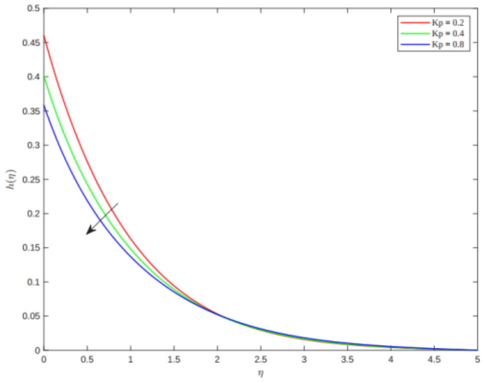

Figure 9. Micro-rotation profile for different Kp values.

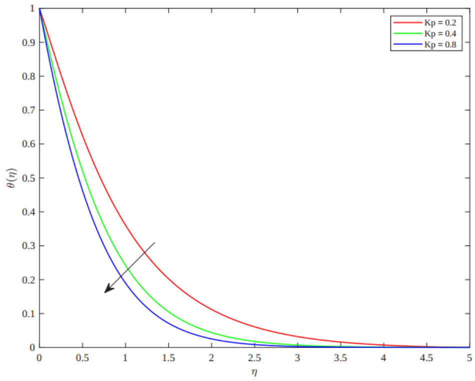

Figure 10. Temperature profile for different Kp values.

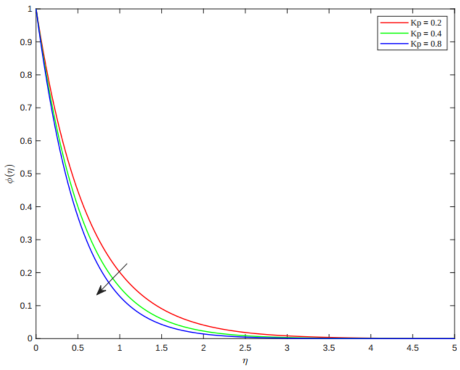

Figure 11. Concentration profile for different Kp values.

The effects of the porosity parameter Kp on the fluid velocity, angular velocity, temperature, and concentration profiles are shown in Figures 8 to 11. Porosity characterizes the medium's permeability. Figure 8 demonstrates that the fluid velocity increases with the increasing values of the porosity parameter. This is because higher porosity means larger permeability, allowing the fluid to flow more easily through the porous medium, reducing resistance and enhancing velocity. Figures 9 to 11 show that increasing the porosity parameter reduces angular velocity, temperature, and concentration profiles. The temperature profile tends to decrease because higher permeability facilitates better heat dissipation, thereby lowering thermal resistance and thinning the thermal boundary layer. Greater porosity allows easier fluid flow, enhancing velocity, while reducing angular velocity, temperature, and concentration by facilitating better heat and mass transfer dissipation.

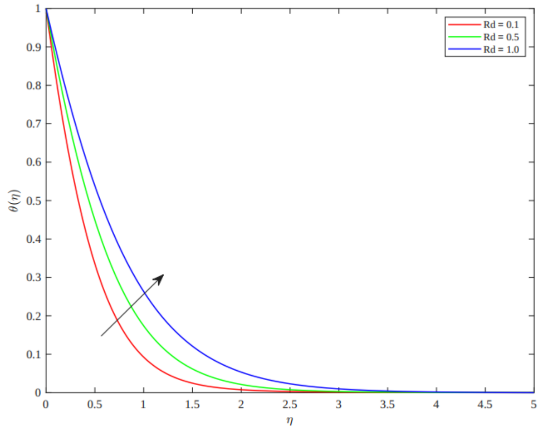

Figure 12. Temperature profile for different Rd values.

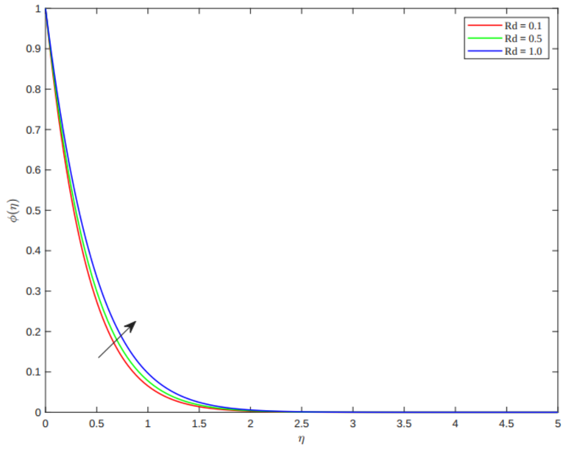

Figure 13. Concentration profile for different Rd values.

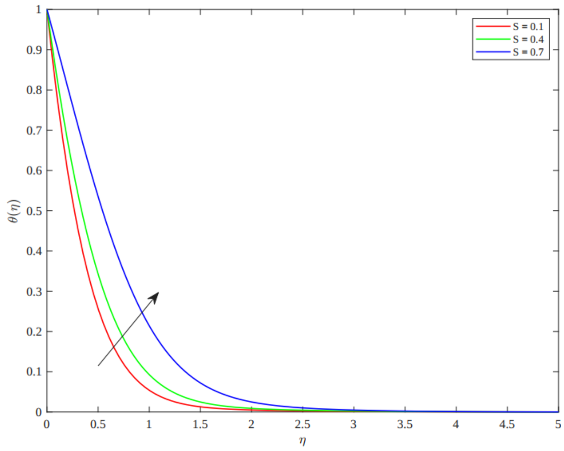

Figure 14. Temperature profile for different S values.

Figures 12 and 13 show how varying the thermal radiation parameter influences temperature and concentration profiles, respectively. Thermal radiation (Rd) represents radiative heat flux in the fluid. Figure 12 demonstrates that the temperature distribution increases as the thermal radiation parameter rises. Higher values of this parameter supply more heat to the fluid, increasing both the temperature and the thickness of the thermal boundary layer. Figure 13 shows that increasing the radiation parameter typically enhances the concentration profile.

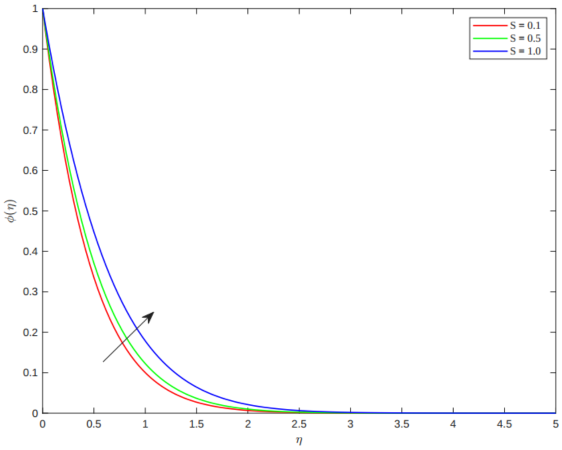

Figure 15. Concentration profile for different S values.

Figures 14 to 15 illustrate how varying the heat source parameter (S) influences the temperature and concentration distributions. The heat-source parameter represents internal heat generation within the fluid. These figures clearly show that both the temperature and concentration profiles increase as the heat source parameter increases. Temperature rises with increasing heat source parameter because a higher value indicates greater internal heat generation within the fluid or medium.

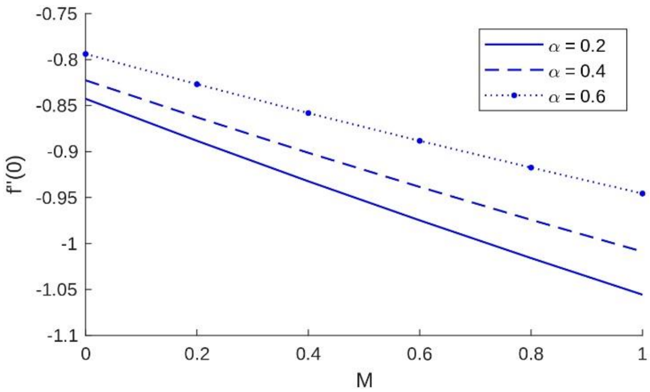

Figure 16. Skin friction coefficient for different M values.

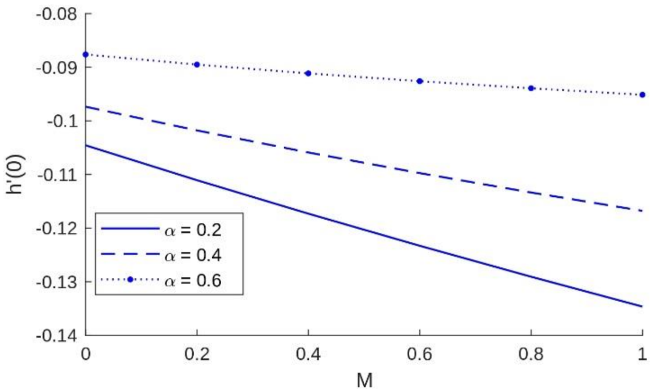

Figure 17. Couple stress coefficient for different M values.

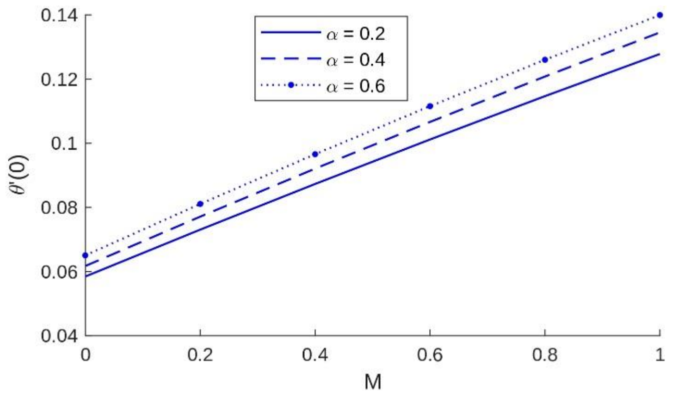

Figure 18. Nusselt number for different M values.

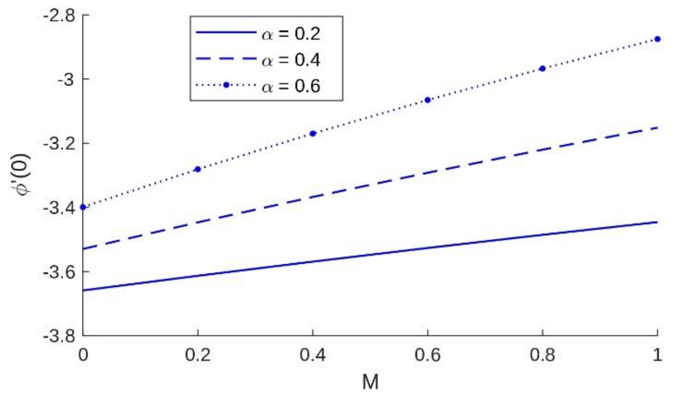

Figure 19. Sherwood number for different M values.

Figures 16 to 19 represent the influence of the magnetic parameter or Hartmann Number (M) and melting parameter (α) on the skin-friction, couple stress coefficient, temperature gradient, and concentration gradient. As shown in Figures 16 and 17, the skin-friction coefficient and couple stress decrease with increasing M, while higher α produces the opposite trend. In contrast, figures 18 and 19 show that the temperature and concentration gradients increase with increasing values of both M and α.

5. Conclusions

This work numerically analyzed the radiative magnetohydrodynamic micropolar boundary-layer flow across an exponentially expanding inclined sheet, accounting for the coupled effects of Joule heating, viscous dissipation, chemical reaction, heat source/sink, porous media, and surface slip. The numerical results were validated against existing literature values, demonstrating excellent agreement with a maximum deviation below 0.03%, thereby confirming the reliability of the computational model. The major conclusions of the study are as follows: the fluid's temperature and concentration increase as the Eckert number (Ec) increases. Additionally, a rise in the chemical reaction parameter (Kc) leads to enhanced angular velocity and temperature profiles, while simultaneously reducing the velocity and concentration profiles. Furthermore, both the temperature and concentration profiles are observed to increase with the heat source parameter (S) and the thermal radiation parameter (Rd). Finally, the surface shear stress is found to be enhanced by increasing both the magnetic parameter and the melting parameter.

Despite its accuracy and strong physical insights, the model assumes a steady-state laminar flow, constant thermo-physical properties, and a low magnetic Reynolds number, which may not capture turbulent or transient industrial processes. Additionally, nonlinear radiative heat transfer and temperature-dependent viscosity effects were not explored.

Future work may incorporate nanoparticles, multiphase effects, viscoelastic or hybrid nanofluid rheology, and machine-learning–assisted surrogate solvers to extend applicability to advanced thermal manufacturing systems.

6. Future Extensions and Research Implications

The outcomes of this investigation provide a foundation for extending the present model toward more realistic physical configurations and experimental validation. Although the numerical results demonstrate consistent behavior across a wide range of governing parameters, including magnetic field strength, chemical reactivity, and thermal radiation, the current formulation is restricted to laminar, steady, two-dimensional boundary-layer flow with constant thermophysical properties. Future studies may explore unsteady and turbulent regimes, variable thermal conductivity, or temperature-dependent viscosity to better reflect real-world micropolar fluid applications. Additionally, incorporating nanoparticle suspensions, hybrid fluids, or nonlinear radiative heat transfer laws may further enhance the model's applicability in biomedical, nuclear cooling, and polymer manufacturing systems. Experimental validation—particularly using controlled magnetohydrodynamic setups or micro-scale rheological measurement techniques would strengthen the reliability of the predictions and provide empirical bounds on the deviation observed between theoretical and measured values. Machine learning–assisted surrogate modeling may also be developed to accelerate optimization and sensitivity analysis for industrial-scale thermal design and heat exchanger systems.

Author Contributions

Conceptualization, K.B. and S.C.; methodology, S.A and J.K.; software, K.B. and J.K.; validation, K.B., S.C., and S.A.; formal analysis, K.B. and S.A.; investigation, K.B., S.C.; writing—original draft preparation, K.B. and J.K.; writing—review and editing, K.B., S.A. and S.C.; visualization, K.B.; supervision, S.C. and J.K. All authors have read and agreed to the published version of the manuscript.

Institutional Review Board Statement

Not applicable.

Informed Consent Statement

Not applicable.

Data Availability Statement

Data supporting the findings of this study are available upon reasonable request from the corresponding author.

Funding

This research received no external funding.

Acknowledgments

The authors would like to thank Gauhati University, Guwahati, Assam, India.

Conflicts of Interest

The authors declare no conflict of interest.

Abbreviations

The following abbreviations are used in this manuscript:

Abbreviation	Definition
x, y	Cartesian Coordinates Along and Normal to the Stretching Sheet
u, v	Velocity Components in the (x)- and (y)-directions
$\psi(x, y)$	Stream Function
$N(x, y)$	Micro-rotation Function
$T(x, y)$	Fluid Temperature
$C(x, y)$	Concentration of Species
η	Similarity Variable
$h(\eta)$	Dimensionless Micro-rotation
$\theta(\eta)$	Dimensionless Temperature
$\phi(\eta)$	Dimensionless Concentration
ρ	Fluid Density
μ	Dynamic Viscosity
ν	Kinematic Viscosity
κ	Vortex Viscosity
γ	Spin-gradient Viscosity
j	Micro-inertia Density
k	Thermal Conductivity
C_p	Specific Heat at Constant Pressure
D	Molecular Diffusivity
σ	Electrical Conductivity
β_T	Thermal Expansion Coefficient
β_C	Volumetric Expansion Coefficient for Concentration
$B(x)$	Applied Magnetic Field
g	Acceleration due to Gravity
Ω	Inclination Angle of the Sheet
σ^*	Stefan–Boltzmann Constant
k^*	Mean Absorption Coefficient
Q	Heat Source/Sink Coefficient
k_0	First-order Chemical Reaction Rate Constant
u_w	Stretching Surface Velocity
T_w	Surface Temperature
T_∞	Ambient/Free-Stream Temperature
C_w	Concentration at the Surface
C_∞	Ambient Concentration
λ	Latent Heat of Fusion
C_s	Surface Heat Capacity
χ	Slip Coefficient
M	Hartmann Number
K	Material Parameter
K_p	Porosity Parameter

Abbreviation	Definition
Pr	Prandtl Number
Sc	Schmidt Number
Ec	Eckert Number
Rd	Radiation Parameter
S	Non-dimensional Heat Source/Sink Parameter
K_c	Chemical Reaction Parameter
Re_x	Local Reynolds Number
τ_w	Shear Stress at Wall
Nu_x	Local Nusselt Number
C_f	Skin-friction Coefficient
Sh_x	Local Sherwood Number
C_s	Couple Stress Coefficient

References

1 Eringen, A.C. Theory of Micropolar Fluids. *J. Math. Mech.* **1966**, *16*, 1-18.

2. Srivastava, N. MHD Flow of the Micropolar Fluid between Eccentrically Rotating Disks. *Int. Sch. Res. Notices* **2014**, *2014*, 317075, https://doi.org/10.1155/2014/317075.

3. Crane, L.J. Flow past a stretching plate. *J. Appl. Math. Phys.* **1970**, *21*, 645-647, https://doi.org/10.1007/BF01587695.

4. Agrawal, R.; Saini, S.K.; Kaswan, P. Numerical modeling of MHD micropolar fluid flow and melting heat transfer under thermal radiation and Joule heating. *Int. J. Comput. Methods Eng. Sci. Mech.* **2023**, *24*, 143-154, https://doi.org/10.1080/15502287.2022.2113183.

5. Sharma, S.; Dadheech, A.; Parmar, A.; Arora, J.; Al-Mdallal, Q.; Saranya, S. MHD micro polar fluid flow over a stretching surface with melting and slip effect. *Sci. Rep.* **2023**, *13*, 10715, https://doi.org/10.1038/s41598-023-36988-3.

6. Borah, K.; Konch, J.; Chakraborty, S. Numerical Simulation of Soret and Dufour Effects on Micropolar Nanofluid Flow with Swimming Gyrotactic Microorganisms. *Lett. Appl. NanoBioSci.* **2025**, *14*, 64, https://doi.org/10.33263/LIANBS142.064.

7. Abdelgaber, K.M.; Fathy, M.; Abbassi, P.k.; Elbarkoki, R.A. Heat and mass transfer of micropolar fluid flow over a stretching sheet by legendre collocation method. *Sci. Rep.* **2025**, *15*, 25921, https://doi.org/10.1038/s41598-025-10028-8.

8. Lu, D.; Ramzan, M.; Ahmad, S.; Chung, J.D.; Farooq, U. A numerical treatment of MHD radiative flow of Micropolar nanofluid with homogeneous-heterogeneous reactions past a nonlinear stretched surface. *Sci. Rep.* **2018**, *8*, 12431, https://doi.org/10.1038/s41598-018-30965-x.

9. Bilal, M.; Saeed, A.; Gul, T.; Kumam, W.; Mukhtar, S.; Kumam, P. Parametric simulation of micropolar fluid with thermal radiation across a porous stretching surface. *Sci. Rep.* **2022**, *12*, 2542, https://doi.org/10.1038/s41598-022-06458-3.

10. Kausar, M.S.; Al-Sharifi, H.A.M.; Hussanan, A.; Mamat, M. The Effects of Thermal Radiation and Viscous Dissipation on the Stagnation Point Flow of a Micropolar Fluid over a Permeable Stretching Sheet in the Presence of Porous Dissipation. *Fluid Dyn. Mater. Process.* **2023**, *19*, 61–81, https://doi.org/10.32604/fdmp.2023.021590.

11. Saraswathy, M.; Prakash, D.; Durgaprasad, P. MHD Micropolar Fluid in a Porous Channel Provoked by Viscous Dissipation and Non-Linear Thermal Radiation: An Analytical Approach. *Mathematics* **2023**, *11*, 183, https://doi.org/10.3390/math11010183.

12. Shamshuddin, M.D.; Gamar, F.; Salawu, S.O.; Reddy, B.P. Two-phase micropolar nanofluid flow in an isothermal extending porous sheet with heat radiation and chemical interaction: Numerical study. *Partial Differ. Equ. Appl. Math.* **2025**, *14*, 101226, https://doi.org/10.1016/j.padiff.2025.101226.

13. Mohapatra, R.; Pattanayak, H.; Mishra, S.R. Effect of Chemical Reaction on MHD Micropolar Fluid Flow on a Vertical Surface through Porous Media with Heat Source. *Int. J. Innov. Res. Sci. Eng. Technol.* **2015**, *4*, 9103-9115.

14. Singh, K.; Kumar, M. Influence of Chemical Reaction on Heat and Mass Transfer Flow of a Micropolar Fluid over a Permeable Channel with Radiation and Heat Generation. *J. Thermodyn.* **2016**, *2016*, 8307980, https://doi.org/10.1155/2016/8307980.

15. Verma, K.; Borgohain, D.; Sharma, B. Analysis of Chemical Reaction on MHD Micropolar Fluid Flow over a Shrinking Sheet near Stagnation Point with Nanoparticles and External Heat. *Int. J. Heat Technol.* **2021**, *39*, 262–268, https://doi.org/10.18280/ijht.390129.
16. Mukhopadhyay, S. Slip effects on MHD boundary layer flow over an exponentially stretching sheet with suction/blowing and thermal radiation. *Ain Shams Eng. J.* **2013**, *4*, 485–491, https://doi.org/10.1016/j.asej.2012.10.007.
17. Ramzan, M.; Farooq, M.; Hayat, T.; Chung, J.D. Radiative and Joule heating effects in the MHD flow of a micropolar fluid with partial slip and convective boundary condition. *J. Mol. Liq.* **2016**, *221*, 394-400, https://doi.org/10.1016/j.molliq.2016.05.091.
18. Mandal, I.C.; Mukhopadhyay, S.; Vajravelu, K. Melting Heat Transfer of MHD Micropolar Fluid Flow Past An Exponentially Stretching Sheet with SLip and Thermal Radiation. *Int. J. Appl. Comput. Math.* **2021**, *7*, 31, https://doi.org/10.1007/s40819-021-00955-1.
19. Salah, F.; Sidahmed, A.O.M. Chemical Reaction and Radiation Effects on MHD Flow of Oldroyd-B Fluid through Porous Medium Past an Exponentially Stretching Sheet with Heat Sink. *J. Appl. Math.* **2022**, *2022*, 6582295, https://doi.org/10.1155/2022/6582295.
20. Fairul Naim Abu, B.; Siti Khuzaimah, S. MHD Stagnation-Point Flow and Heat Transfer Over an Exponentially Stretching/Shrinking Vertical Sheet in a Micropolar Fluid with a Buoyancy Effect. *J. Adv. Res. Numer. Heat Transf.* **2022**, *8*, 50-55.
21. Mohammed, I.S.; Lavanya, B.; Dharmaiah, G.; Reddy, T.S.; Roja, P. Melting Heat Transfer Effects on MHD Chemically Thermally Radiative Micropolar Fluid Flow Towards Stretching Exponentially Sheet with Heat Sink/Source. *CFD Lett.* **2025**, *17*, 113-129, https://doi.org/10.37934/cfdl.17.7.113129.